Electronic Supplementary Information

Surface engineering of triboelectric nanogenerator for room temperature high-performance self-powered formaldehyde sensor

Chih-Yu Chang,* Yu-Hsuan Cheng, Chun-Yi Ho

Department of Materials Science and Engineering, National Taiwan University of Science and Technology, Taipei, 10607, Taiwan (R.O.C.) (E-mail: cychang@gapps.ntust.edu.tw)

Table S1. XPS binding energy values and surface concentration of bpy-PMA films before and after FA exposure.

Peak component	Mo 3d binding energy [eV]				Mo 3d concentration [at.%]			
	Mo^{6+} $3d_{5/2}$	Mo^{6+} $3d_{7/2}$	Mo^{5+} $3d_{5/2}$	Mo^{5+} $3d_{7/2}$	Mo^{6+} $3d_{5/2}$	Mo^{6+} $3d_{7/2}$	Mo^{5+} $3d_{5/2}$	Mo^{5+} $3d_{7/2}$
Before sensing	233.4	236.5	N.A.	N.A.	40.68	59.32	N.A.	N.A.
After sensing	233.3	236.4	235.4	231.7	11.06	27.16	23.18	38.60

Table S2. Comparison of the characteristics of state-of-the-art gas sensors based on monolithic TENG previously reported as well as the present work.

Source	Materials	Target gas	Selectivity[a]	Response time [sec][a]	Power density [W m^{-2}][a]	Power [mW][a]
Ref. 1	PDMS PANI with Ce-doped ZnO	NH_3	—	—	—	—
Ref. 2	PANI PVDF	NH_3	—	40	—	—
Ref. 3	PDMS PEI	CO_2	—	—	—	—
Ref. 4	PEI FEP	CO_2	—	—	—	—
Ref. 5	PET ITO with Pd deposition	H_2	—	1800	—	—
Ref. 6	PI MC	H_2	—	82 to 88	—	—
Ref. 7	Latex Synthesized material	NO_2	—	—	—	—
Ref. 8	ZnO-doped Ag PDMS	Acetylene	—	—	—	0.18
Ref. 9	Al rGO-In_2O_3	Aniline	—	350	—	—
This work	PTZ/Ag NPs PDMS/bpy-PMA	Formaldehyde	130	4.65	2.97[b] or 8.93[c]	1.19[b] or 3.57[c]

[a] "—" in the table implies that the data are not recorded in research.
[b] The dielectric layer is PDMS planar film functionalized with bpy-PMA.
[c] The dielectric layer is PDMS nanopillar arrays functionalized with bpy-PMA.

Table S3. Comparison of the charactersitics of state-of-the-art FA sensors previously reported as well as the present work.

Source	Sensing materials	Self-powered mode	Working temperature [°C]	Selectivity[a]	Response time [sec][a]
Ref. 10	SnO_2/rGO nanocomposites	No	160	—	<10 (<25 ppm)
Ref. 11	Zn_2SnO_4/SnO_2 hierarchical sructure	No	200	—	76 (20 ppm)
Ref. 12	rGO/$ZnSnO_3$ microspheres	No	103	—	31 (10 ppm)
Ref. 13	ZnO@ZIF-8 nanorod	No	300	4	14 (100 ppm)
Ref. 14	ZnO micro-octahedrons	No	400	—	<46 (200 ppm)
Ref. 15	In_2O_3 hierarchical architecurets	No	260	—	1 (100 ppm)
Ref. 16	Ag-ZnO nanocomposites	No	240	—	12 (100 ppm)
Ref. 17	SnO_2 nanosheets	No	200	101	30 (200 ppm)
Ref. 18	rGO/TiO_2 nanosheet	No	≈25	—	65 (0.5 ppm)
Ref. 19	SnO_2 with lamellar and plicated membranes	No	200	—	50 (10 ppm)
Ref. 20	Co_3O_4/ZnO hollow spheres with nanoparticles	No	160	—	—
Ref. 21	VG/SnO_2 nanoparticles	No	≈25	—	46 (5 ppm)
Ref. 22	Ga-In bimetallic oxide nanofibers	No	150	—	1 to 14 (100 to 0.2 ppm)
Ref. 23	Co_3O_4/ZnO core-shell nanofibers	No	220	—	6 (100 ppm)
Ref. 24	NiO/SnO_2 microspheres	No	200	—	—
Ref. 25	Ni-SnO_2 nanoparticles	No	200	—	18 (50 ppm)
Ref. 26	SnO/SnO_2 nano-flowers assemble from nanosheets	No	120	33	7 (50 ppm)
Ref. 27	NiO-SnO_2 microflowers	No	100	—	—
Ref. 28	Co-rich $ZnCo_2O_4$ hollow nanospheres	No	225	—	—
Ref. 29	ZnO nanopowders	No	210	—	340 (0.01 ppm)
Ref. 30	Li-doped NiO	No	600	—	—
Ref. 31	CdO activated Sn doped ZnO	No	200	—	<300 (32 ppm)
Ref. 32	Ga doped ZnO	No	400	130	180 (32 ppm)
This work	PDMS/bpy-PMA	Yes	25		4.65 (1 ppm)

[a] "—" in the table implies that the data are not recorded in research.

Table S4. Comparison of the characteristics of state-of-the-art breath sensors previously reported as well as the present work.

Source	Biomarker gas	Disease	Materials	Self-powered mode	Working temperature [°C]	Selectivity[a]	Response time [sec]
Ref. 33	NO	Asthma	Single walled CNTs	No	≈25	—	255 (485 ppb)
Ref. 34	NO_2	Asthma	Electrochemical, etc	No	250	—	63 (5 ppm)
Ref. 35	Acetone	Diabetes	Ce-ZnO based	No	≈25	—	20 (100 ppm)
Ref. 36	H_2S	Halitosis	α-Fe_2O_3	No	350	130	30 (50 ppm)
This work	Formaldehyde	Lung cancer	PDMS/bpy-PMA	Yes	25		4.65 (1 ppm)

[a] "—" in the table implies that the data are not recorded in research.

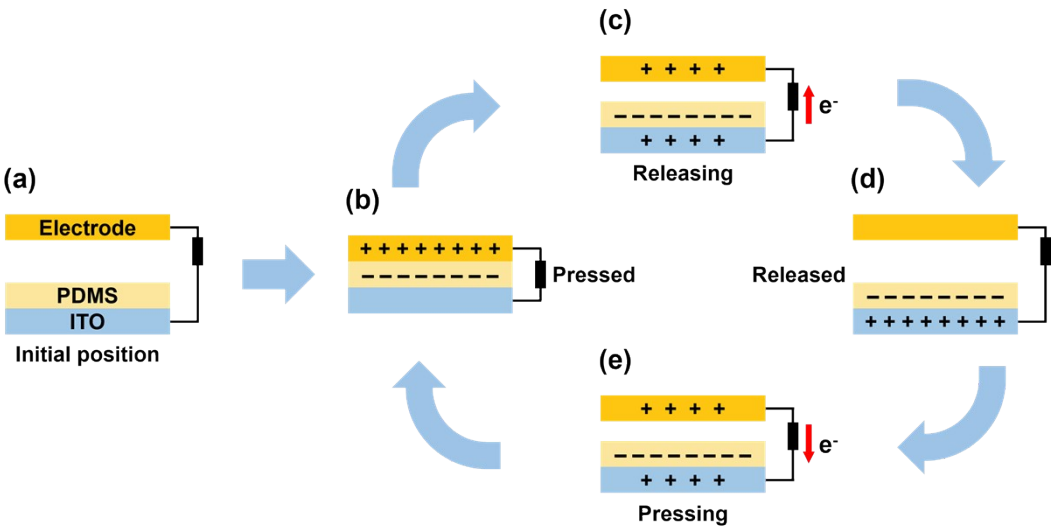

Fig. S1. Schematic illustration of working principle of electrode-to-dielectric vertical contact-separation mode TENG.

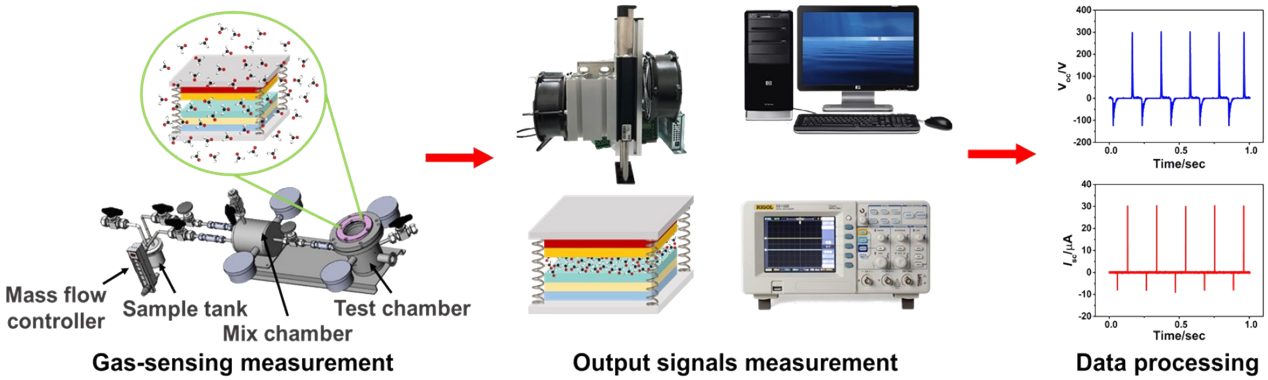

Fig. S2. Schematic illustration of the experimental setup for FA sensing.

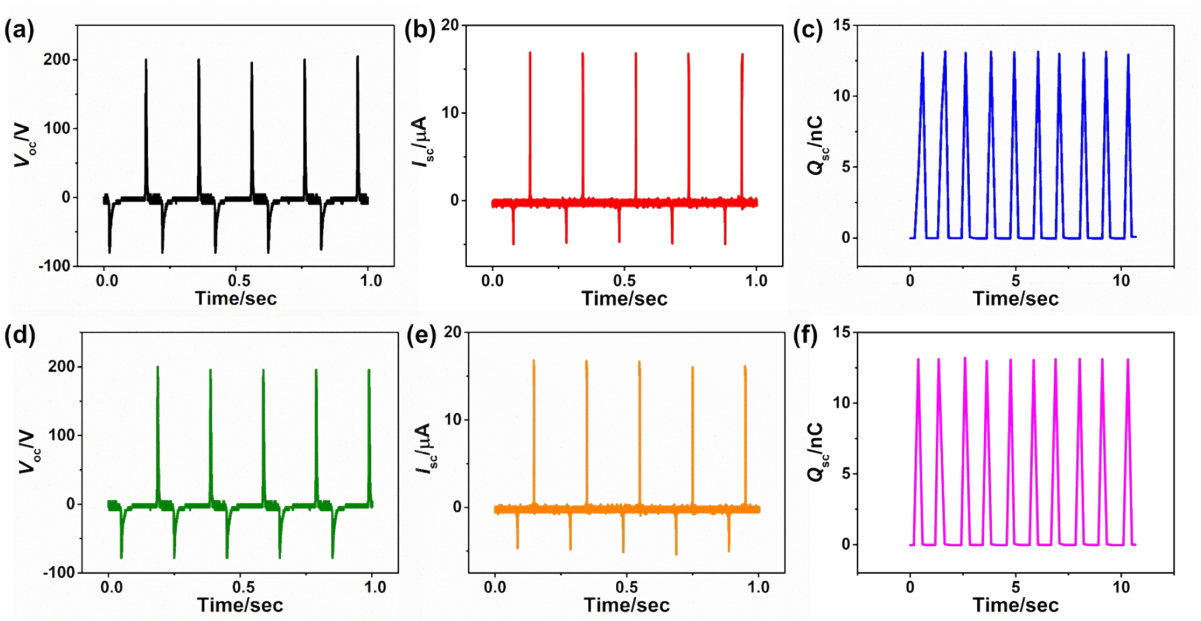

Fig. S3. Output characterization of PDMS-based TENG before (a-c) and after (d-f) FA exposure: V_{oc} (a, d), I_{sc}, (b, e), and Q_{sc} (c, f).

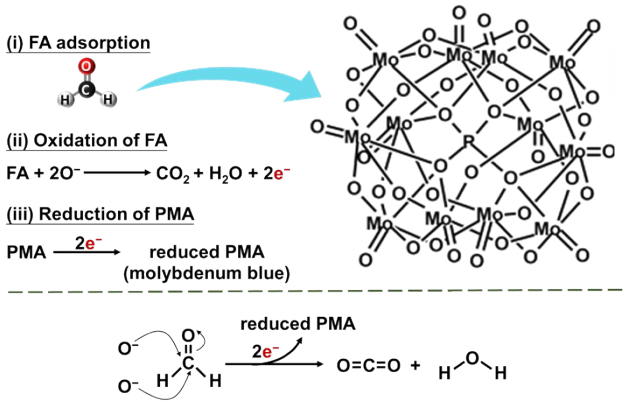

Fig. S4. The schematic illustration of the possible sensing mechanism of FA gases by PMA

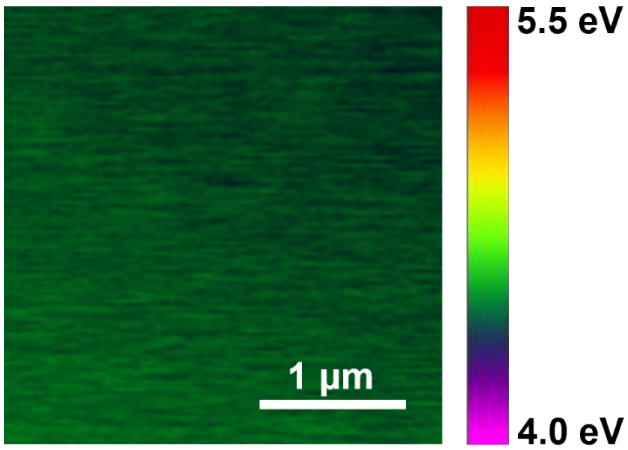

Fig. S5. KPFM image of PDMS/PMA film after FA exposure.

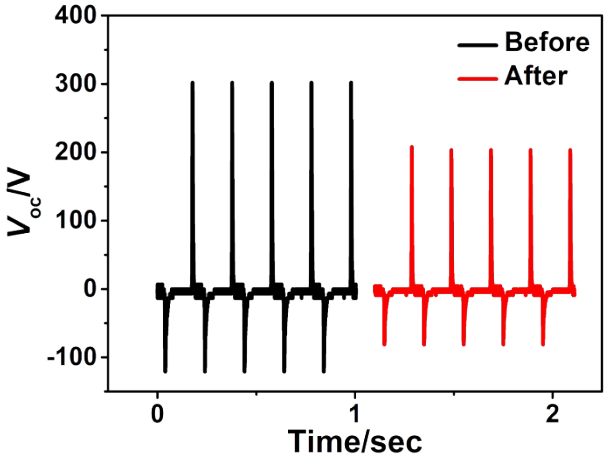

Fig. S6. V_{oc} output of the TENG (dielectric layer: PDMS/PMA, electrode: ITO/PEI) before and after exposure to high humidity atmosphere (relatively humidity ≈90%) for 1 hr.

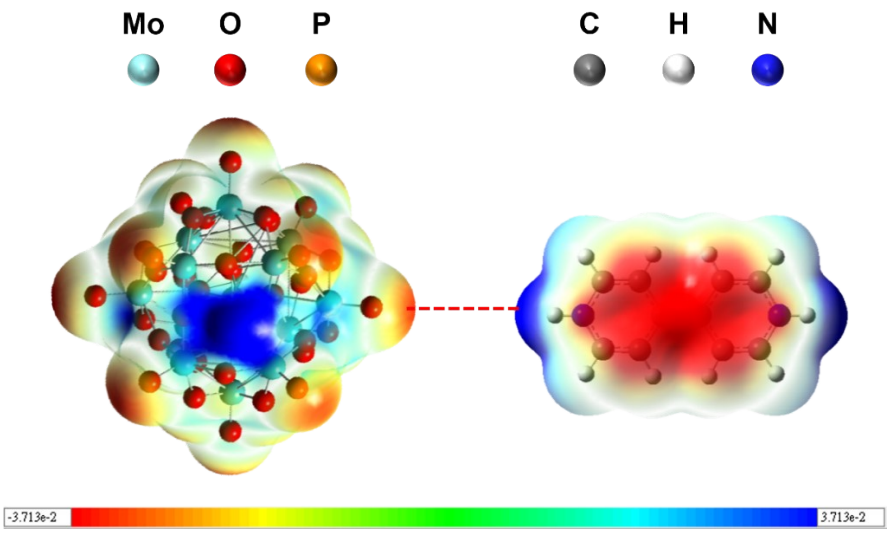

Fig. S7. Guassian-calculated ESP maps of PMA anions and pyridinium (dashed line indicates the electrostatic force between the electronegative oxygen atoms of PMA anions and ammonium atoms of pyridinium).

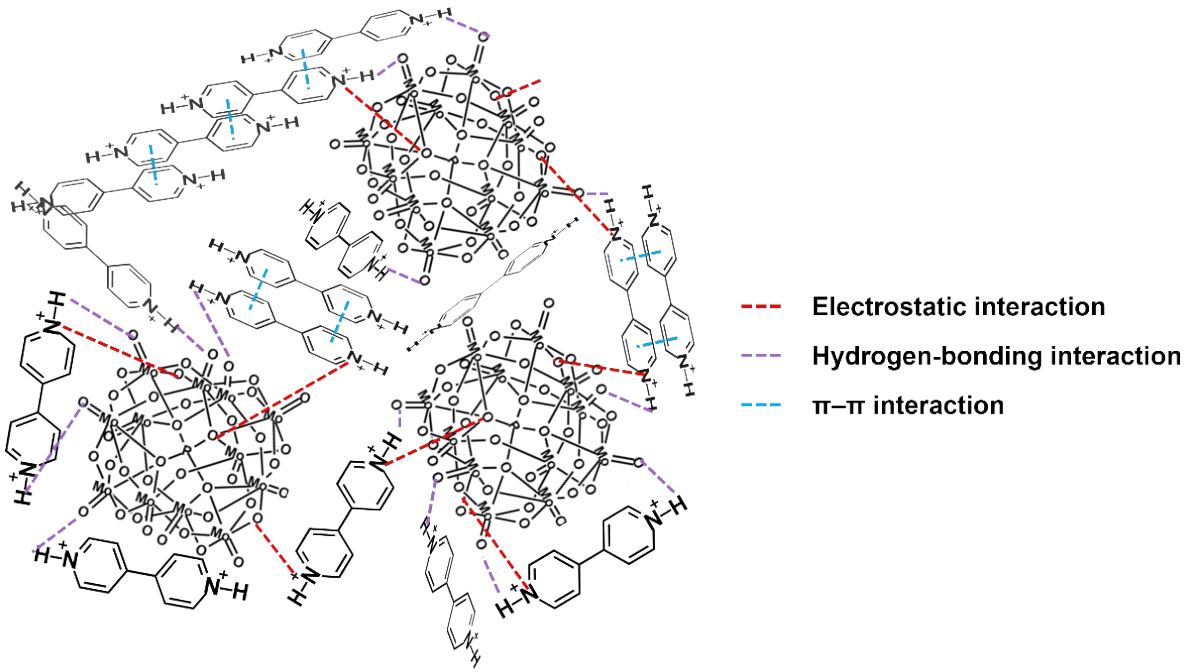

Fig. S8. Schematic representation of the possible interaction between PMA anions and pyridinium.

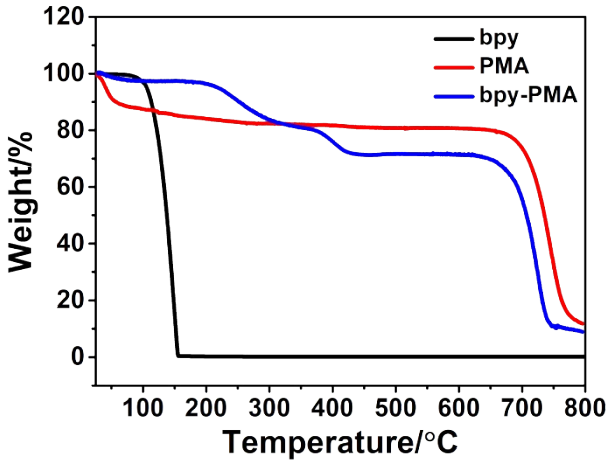

Fig. S9. Thermogravimetric analysis of bpy, PMA, and bpy-PMA.

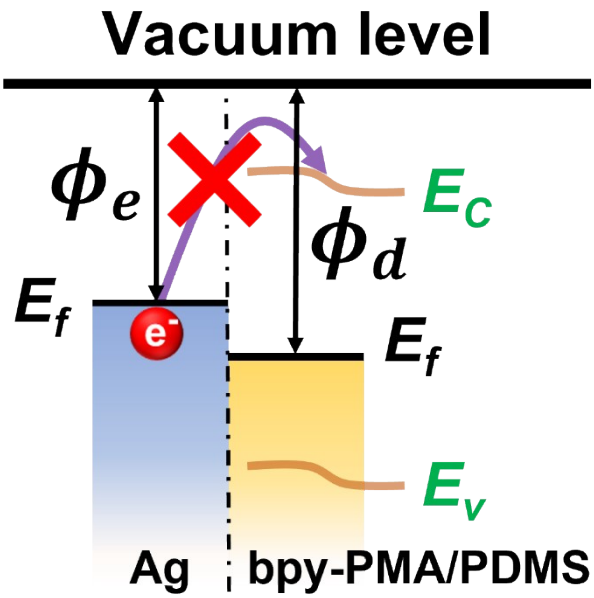

Fig. S10. Schematic energy level diagram of Ag electrode and PDMS/bpy-PMA dielectric layer. Φ_e, Φ_d, E_f, E_c, and E_v represent the work-function of electrode, work-function of dielectric layer, Fermi energy level, conduction band edge, and valence band edge, respectively.

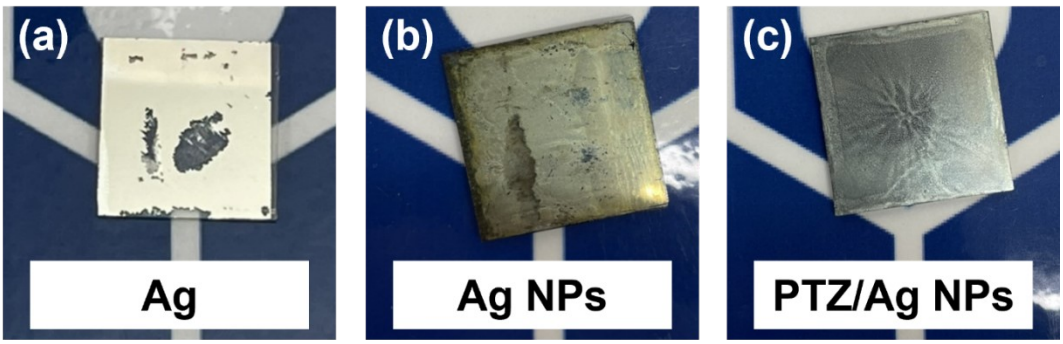

Fig. S11. Photographs of various electrode layers after 200,000 times of contact-separation operation.

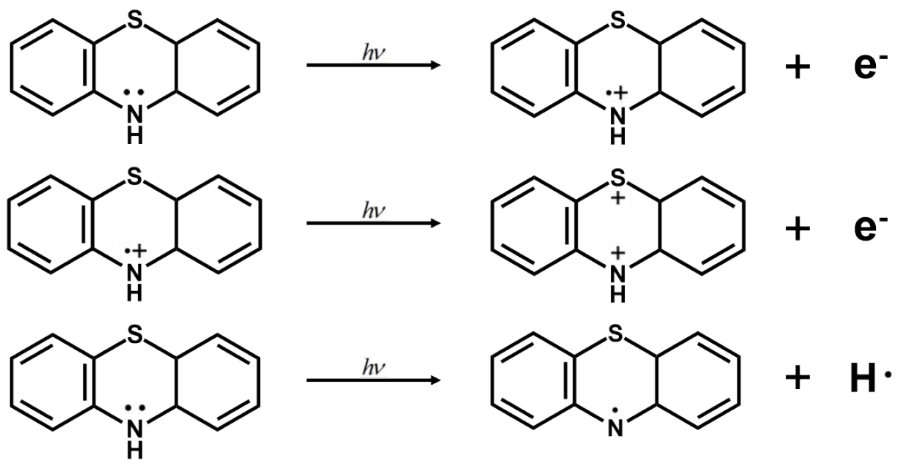

Fig. S12. Proposed mechanism for the photo-initiated reactions of PTZ.

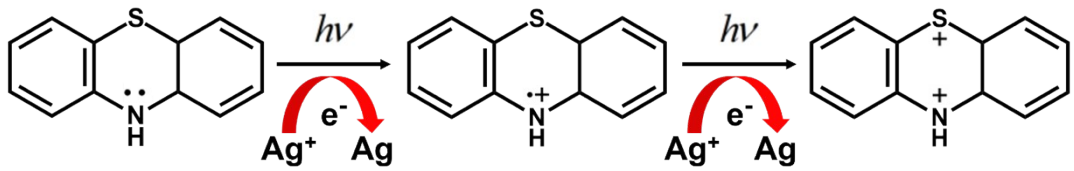

Fig. S13. Schematic representation of photoinduced reduction of Ag^+ ions to Ag by PTZ.

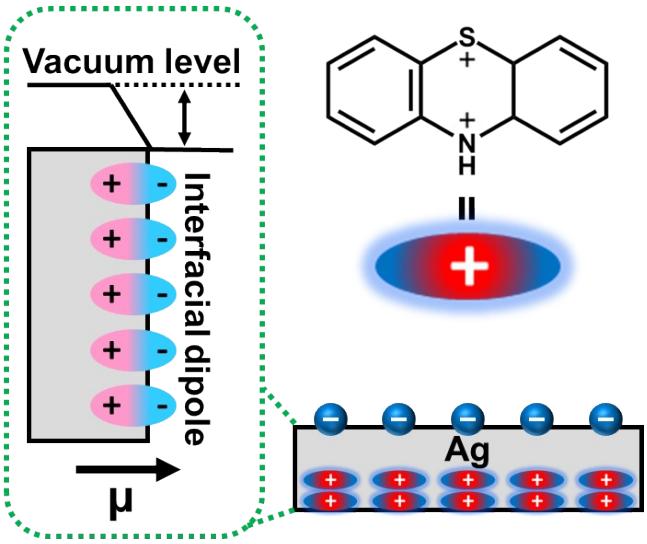

Fig. S14. Schematic illustration of WF modulation of Ag NPs film via PTZ modification

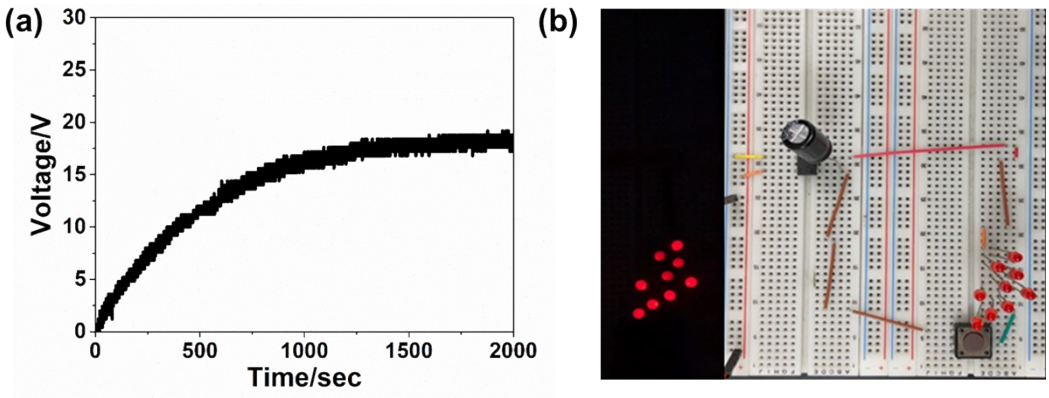

Fig. S15. (a) Charging curve of a capacitor connected to TENG with the rectifying circuit. (b) A photograph of commercial LEDs lit up simultaneously by charging a capacitor from the TENG.

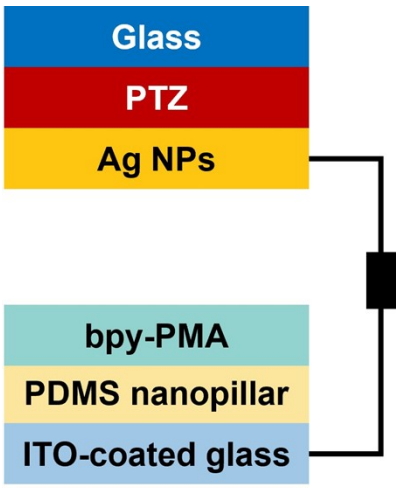

Fig. S16. Schematic illustration of the TENG architecture with PDMS nanopillar arrays.

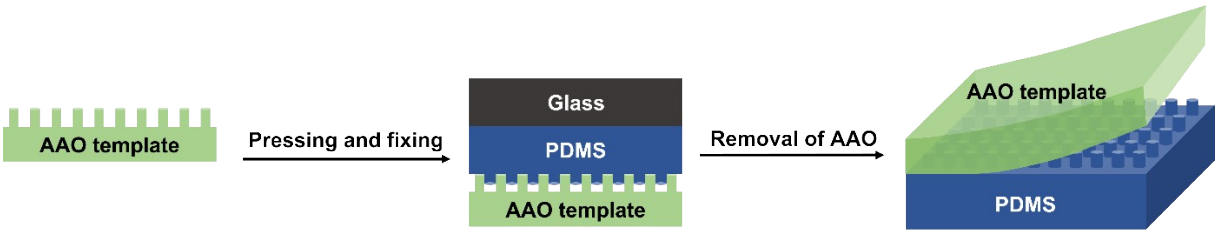

Fig. S17. Schematic illustration of the fabrication procedures for PDMS nanopillars via AAO template-assisted method.

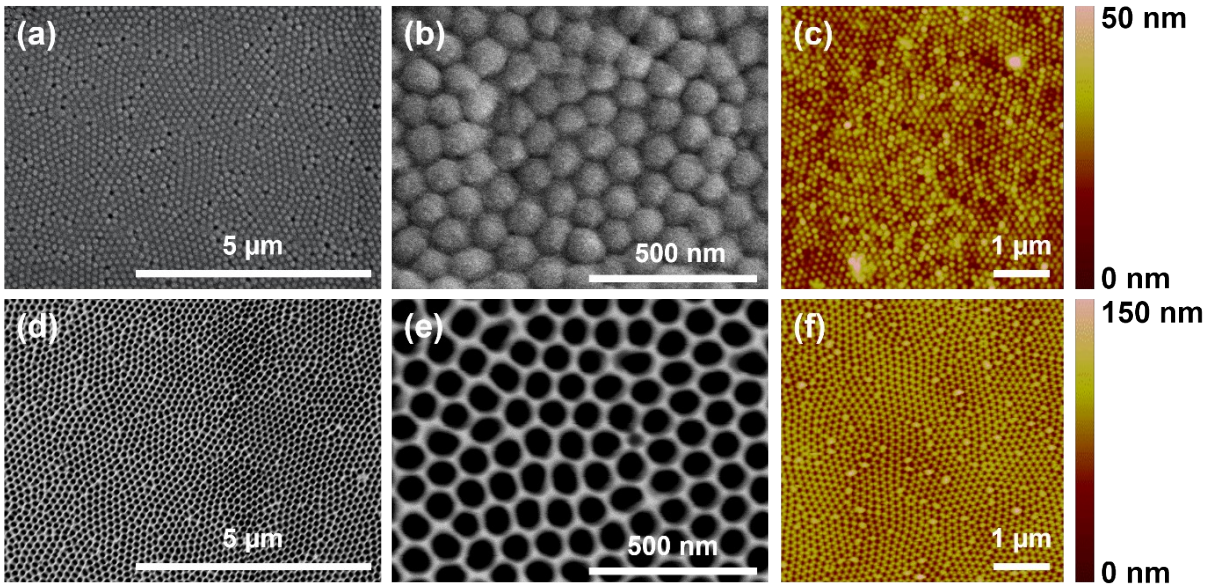

Fig. S18. (a, b, d, e) Top-view SEM images, and (c, f) AFM topographic images of: PDMS nanopillars (a-c), and bare AAO template (d-f).

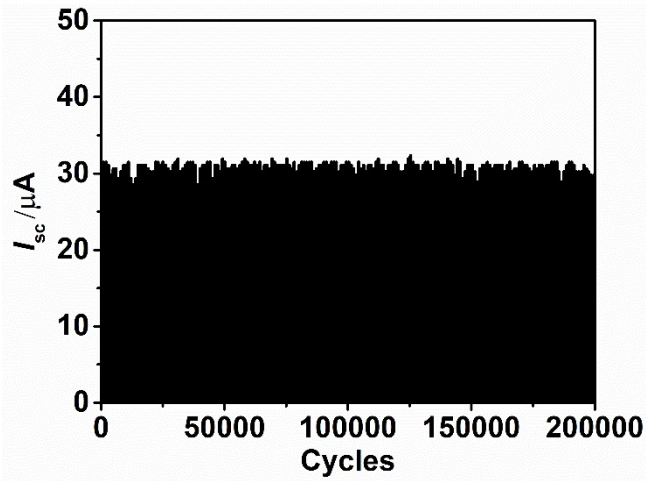

Fig. S19. Evolution of I_{sc} of TENG as a function of continuous operating cycles.

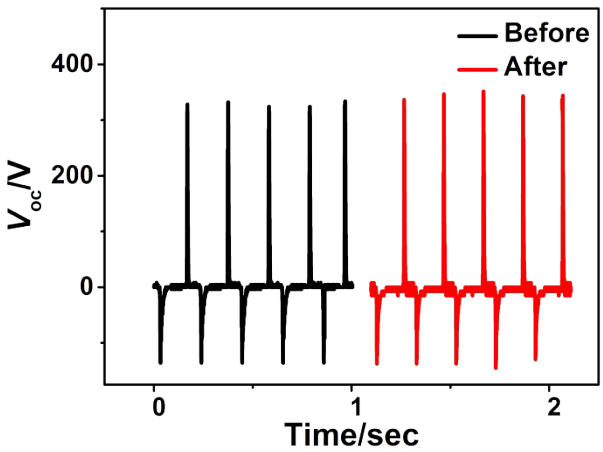

Fig. S20. V_{oc} output of the TENG (dielectric layer: PDMS/bpy-PMA, electrode: PTZ/Ag NPs) before and after exposure to high humidity condition (relatively humidity ≈90%) for 1 hr.

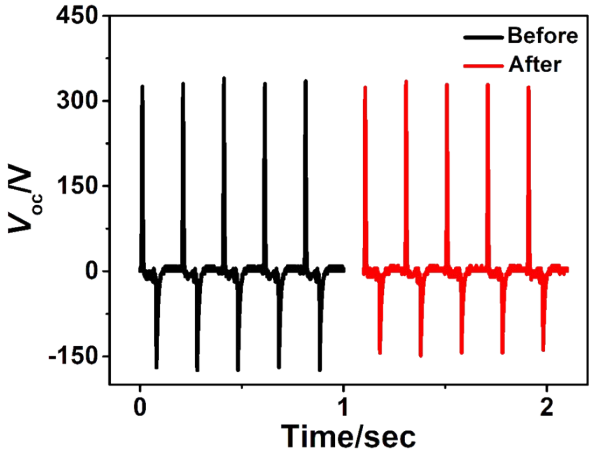

Fig. S21. V_{oc} output of the TENG (dielectric layer: PDMS/bpy-PMA, electrode: PTZ/Ag NPs) before and after immersion in water for 12 hr.

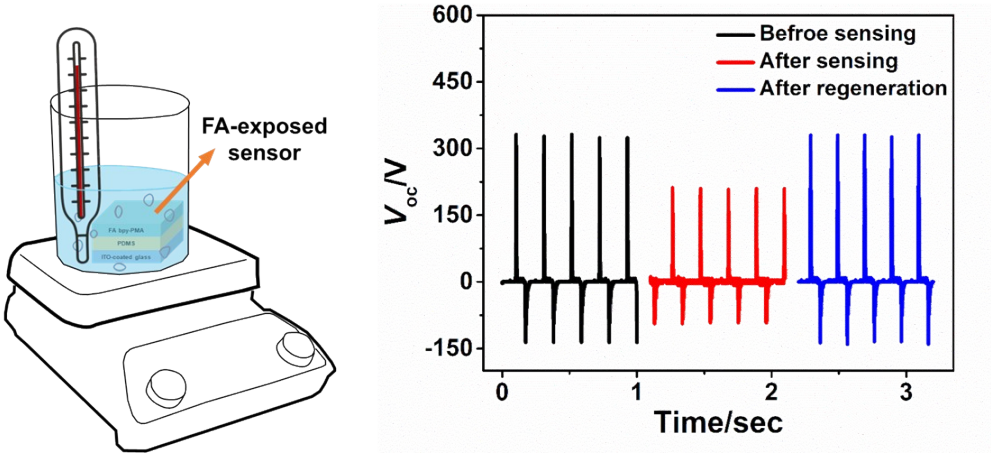

Fig. S22. Schematic illustration of the experimental setup used for regeneration of the active sensing layer (left panel) and V_{oc} output of the TENG (dielectric layer: PDMS/bpy-PMA, electrode: PTZ/Ag NPs) measued under different conditions (right panel).

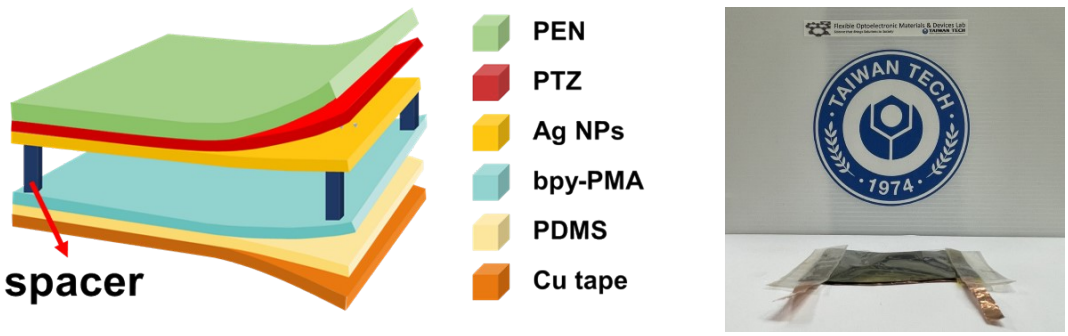

Fig. S23. Schematic illustration of the device architecture of flexible TENG (left panel) and a photograph of flexible TENG (right panel).

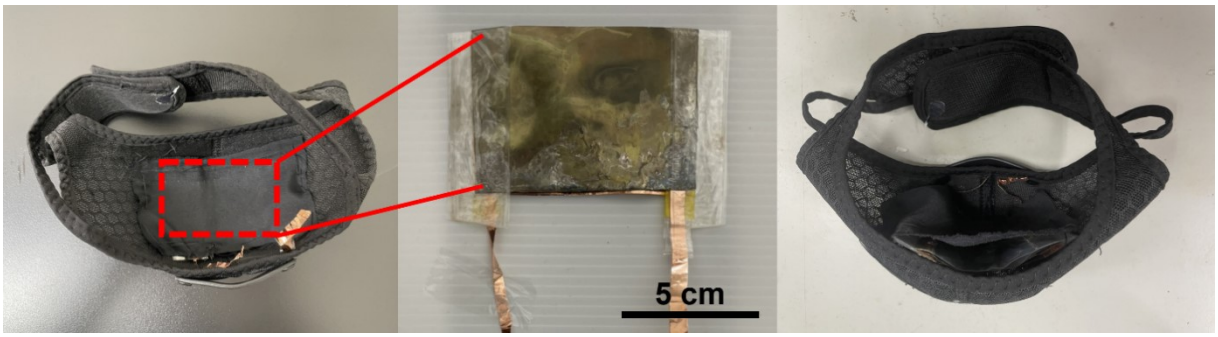

Fig. S24. Photographs of self-powered face mask based on flexible TENG (note: bending radius of flexible TENG = 13 mm).

Fig. S25. A photograph of as-fabricated TENG.

References

1. S. Wang, H. Tai, B. Liu, Z. Duan, Z. Yuan, H. Pan, Y. Su, G. Xie, X. Du and Y. Jiang, *Nano Energy*, 2019, **58**, 312-321.
2. S. Cui, Y. Zheng, T. Zhang, D. Wang, F. Zhou and W. Liu, *Nano Energy*, 2018, **49**, 31-39.
3. H. Wang, H. Wu, D. Hasan, T. He, Q. Shi and C. Lee, *ACS Nano*, 2017, **11**, 10337-10346.
4. I. Kim, H. Roh and D. Kim, *Nano Energy*, 2019, **65**, 103990.
5. S.-H. Shin, Y. H. Kwon, Y.-H. Kim, J.-Y. Jung and J. J. N. Nah, 2016, **6**, 186.
6. A. S. M. I. Uddin and G.-S. Chung, *Sens. Actuators B Chem.*, 2017, **245**, 1-10.
7. Y. Su, J. Wang, B. Wang, T. Yang, B. Yang, G. Xie, Y. Zhou, S. Zhang, H. Tai, Z. Cai, G. Chen, Y. Jiang, L.-Q. Chen and J. Chen, *ACS Nano*, 2020, **14**, 6067-6075.
8. A. S. M. I. Uddin, U. Yaqoob and G.-S. Chung, *ACS Appl. Mater. Interfaces*, 2016, **8**, 30079-30089.
9. J. Chang, H. Meng, C. Li, J. Gao, S. Chen, Q. Hu, H. Li and L. Feng, *Adv. Mater. Technol.*, 2020, **5**, 1901087.
10. X. Rong, D. Chen, G. Qu, T. Li, R. Zhang and J. Sun, *Sens. Actuators B Chem.*, 2018, **269**, 223-237.
11. S. Shu, M. Wang, W. Yang and S. Liu, *Sens. Actuators B Chem.*, 2017, **243**, 1171-1180.
12. J. Sun, S. Bai, Y. Tian, Y. Zhao, N. Han, R. Luo, D. Li and A. Chen, *Sens. Actuators B Chem.*, 2018, **257**, 29-36.
13. H. Tian, H. Fan, M. Li and L. Ma, *ACS Sensors*, 2016, **1**, 243-250.
14. L. Zhang, J. Zhao, H. Lu, L. Gong, L. Li, J. Zheng, H. Li and Z. Zhu, *Sens. Actuators B Chem.*, 2011, **160**, 364-370.
15. S. Wang, J. Cao, W. Cui, L. Fan, X. Li and D. Li, *Sens. Actuators B Chem.*, 2018, **255**, 159-165.
16. X. Xing, X. Xiao, L. Wang and Y. Wang, *Sens. Actuators B Chem.*, 2017, **247**, 797-806.
17. R. Xu, L.-X. Zhang, M.-W. Li, Y.-Y. Yin, J. Yin, M.-Y. Zhu, J.-J. Chen, Y. Wang and L.-J. Bie, *Sens. Actuators B Chem.*, 2019, **289**, 186-194.
18. Z. Ye, H. Tai, T. Xie, Z. Yuan, C. Liu and Y. Jiang, *Sens. Actuators B Chem.*, 2016, **223**, 149-156.
19. C. Zhang, J. Wang, R. Hu, Q. Qiao and X. Li, *Sens. Actuators B Chem.*, 2016, **222**, 1134-1143.
20. S. Bai, J. Guo, X. Shu, X. Xiang, R. Luo, D. Li, A. Chen and C. C. Liu, *Sens. Actuators B Chem.*, 2017, **245**, 359-368.
21. Z. Bo, M. Yuan, S. Mao, X. Chen, J. Yan and K. Cen, *Sens. Actuators B Chem.*, 2018, **256**, 1011-1020.
22. H. Chen, J. Hu, G.-D. Li, Q. Gao, C. Wei and X. Zou, *ACS Appl. Mater. Interfaces*, 2017, **9**, 4692-4700.
23. X. Gao, F. Li, R. Wang and T. Zhang, *Sens. Actuators B Chem.*, 2018, **258**, 1230-1241.
24. C. Gu, Y. Cui, L. Wang, E. Sheng, J.-J. Shim and J. Huang, *Sens. Actuators B Chem.*, 2017, **241**, 298-307.
25. J. Hu, T. Wang, Y. Wang, D. Huang, G. He, Y. Han, N. Hu, Y. Su, Z. Zhou, Y. Zhang and Z. Yang, *Sens. Actuators B Chem.*, 2018, **263**, 120-128.
26. N. Li, Y. Fan, Y. Shi, Q. Xiang, X. Wang and J. Xu, *Sens. Actuators B Chem.*, 2019, **294**, 106-115.
27. D. Meng, D. Liu, G. Wang, Y. Shen, X. San, M. Li and F. Meng, *Sens. Actuators B Chem.*, 2018, **273**, 418-428.
28. H. J. Park, J. Kim, N.-J. Choi, H. Song and D.-S. Lee, *ACS Appl. Mater. Interfaces*, 2016, **8**, 3233-3240.
29. X. Chu, T. Chen, W. Zhang, B. Zheng and H. Shui, *Sens. Actuators B Chem.*, 2009, **142**, 49-54.
30. J. A. Dirksen, K. Duval and T. A. Ring, *Sens. Actuators B Chem.*, 2001, **80**, 106-115.
31. N. Han, X. Wu, D. Zhang, G. Shen, H. Liu and Y. Chen, *Sens. Actuators B Chem.*, 2011, **152**, 324-329.
32. N. Han, Y. Tian, X. Wu and Y. Chen, *Sens. Actuators B Chem.*, 2009, **138**, 228-235.
33. E. I. Ionete, S. I. Spiridon, B. F. Monea and E. J. S. Stratulat, *Sensors,* 2019, **19**, 1116.
34. Y.-S. Shim, H. G. Moon, D. H. Kim, L. Zhang, S.-J. Yoon, Y. S. Yoon, C.-Y. Kang and H. W. Jang, *RSC Adv.*, 2013, **3**, 10452-10459.
35. A. J. Kulandaisamy, V. Elavalagan, P. Shankar, G. K. Mani, K. J. Babu and J. B. B. Rayappan, *Ceram. Int.*, 2016, **42**, 18289-18295.
36. Z. Wu, Z. Li, H. Li, M. Sun, S. Han, C. Cai, W. Shen and Y. Fu, *ACS Appl. Mater. Interfaces*, 2019, **11**, 12761-12769.